Neutron diffraction study of the inverse spinels Co_2TiO_4 and Co_2SnO_4

S. Thota[1*], M. Reehuis[2*], A. Maljuk[3], A. Hoser[2], J.-U. Hoffmann[2], B. Weise[3], A. Waske[3], M. Krautz[3], D. C. Joshi[1], S. Nayak[1], S. Ghosh[1], P. Suresh[4], S. Wurmehl[3], O. Prokhnenko[2], and B. Büchner[3].

[1]*Department of Physics, Indian Institute of Technology, Guwahati-781039, Assam, India.*
[2]*Helmholtz-Zentrum Berlin für Materialien und Energie, Hahn-Meitner-Platz 1, D-14109 Berlin, Germany.*
[3]*Leibniz Institute for Solid State and Materials Research, IFW-Dresden, D-01069 Dresden, Germany.*
[4]*Department of Physics, Indian Institute of Science, Bangalore-560012, India*

Abstract

We report a detailed single-crystal and powder neutron diffraction study of Co_2TiO_4 and Co_2SnO_4 between the temperatures 1.6 K and 80 K to probe their spin structures in the ground state. For both compounds the strongest magnetic intensity was observed for the $(111)_M$ reflection due to ferrimagnetic ordering, which sets in below T_N = 48.6 K and 41 K for Co_2TiO_4 and Co_2SnO_4, respectively. An additional low intensity magnetic reflection $(200)_M$ was noticed in Co_2TiO_4 due to the presence of an additional weak antiferromagnetic component. Interestingly, from both the powder and the single-crystal neutron data of Co_2TiO_4 we noticed a significant broadening of the magnetic $(111)_M$ reflection, possibly results from the disordered character of the Ti and Co atoms on the *B* site. Practically, the same peak broadening was found for the neutron powder data of Co_2SnO_4. On the other hand, from our single-crystal neutron diffraction data of Co_2TiO_4 we found a spontaneous increase of particular nuclear Bragg reflections below the magnetic ordering temperature. Our data analysis showed that this unusual effect can be ascribed to the presence of anisotropic extinction, which is associated to a change of the mosaicity of the crystal. In this case it can be expected that competing Jahn-Teller effects act along different crystallographic axes can induce anisotropic local strain. In fact, for both ions Ti^{3+} and Co^{3+} the $2t_g$ levels split into a lower d_{xy} level and yields a higher two-fold degenerate d_{xz}/d_{yz} level. As a consequence, one can expect a tetragonal distortion in Co_2TiO_4 with $c/a < 1$, which could not significantly detected in the present work.

Authors to whom correspondence should be addressed
Email: subhasht@iitg.ac.in & reehuis@helmholtz-berlin.de

I. INTRODUCTION

Magnetic properties of oxides with spinel crystal structure [$AB_2O_4 = A^{2+}(B^{3+})_2O_4$ for normal spinels, and $B^{3+}(A^{2+}B^{3+})O_4$ for inverse spinels] have been the subject of extensive research because of their unusual magnetic behavior and wide variety of applications in high-frequency electronic components such as transformers, tunable noise filters, and magnetic read-write heads [1-10]. Substitution of non-magnetic elements (dilution) inside these oxides at tetrahedral (A) or octahedral (B) sites often induces disorder or lattice distortions. Such issues may generate new pathways of magnetic interactions leading to some complex ferrimagnetic ordering with altered ground state [11-18] and brings about some interesting magnetic phenomena like reentrant spin-glass characteristics, magnetic frustration and bipolar exchange bias [19-29].

Among various classes of spinel compounds that exhibit above properties, cobalt orthotitanate (Co_2TiO_4), cobalt-zinc titanates ($Co_{2-y}Zn_yTiO_4$), cobalt-germanium titanates ($Co_2Ge_xTi_{1-x}O_4$) and cobalt orthostannate (Co_2SnO_4) are some of the best known ferrimagnetic systems which exhibits glassy behavior just below T_N [30-38]. The magnetic ordering in these compounds has already been studied by several authors in polycrystalline form [22-25, 32-38]. In this work we focus on the neutron diffraction studies of Co_2TiO_4 [$(Co^{2+})[Co^{3+}Ti^{3+}]O_4$] together with the magnetic characterization of a single-crystalline sample and compared the results systematically with the polycrystalline Co_2SnO_4. Let us first recall that both compounds, Co_2TiO_4 and Co_2SnO_4 [$Co^{2+}(Co^{2+}Sn^{4+})O_4$], exhibit ferrimagnetic behavior due to unequal magnetic moments of Co^{2+} ions at the tetrahedral A sites [$\mu(A) = 3.87\ \mu_B$] and octahedral B sites [$\mu(B) = 5.19\ \mu_B$ and $4.91\ \mu_B$ for Co_2TiO_4 and Co_2SnO_4, respectively] [22-25]. The nature of magnetism in polycrystalline Co_2TiO_4 was first investigated by Sakamoto and Yamaguchi in 1962 using temperature dependent remanence and torque measurements [39]. These authors report ferrimagnetic behavior in Co_2TiO_4 with Néel temperature $T_N \sim 53$ K together with displaced hysteresis loops along the magnetization axis at 4.2 K [39]. Further, Ogawa and Waki report the temperature dependence of specific heat $C_P(T)$ in Co_2TiO_4 synthesized by cobalt ammonium sulfate and TiO_2 as precursors [40]. These authors observed a weak anomaly across 49 K in the $C_P(T)$ which is associated to the magnetic transition and reported the Debye temperature $\Theta_D \sim 560$ K with $T^{3/2}$ dependence for $T < 30$ K [40]. Later studies by Hubsch and Gavoille reported a semi spin-glass transition $T_{SG} \sim 46$ K ($< T_N$) in Co_2TiO_4 [32]. According to

this report Co_2TiO_4 undergoes a compensation temperature across 30 K where the two-sublattice magnetizations balance with each other [32]. In 1991 Gavoille *et al*. reported that the random anisotropy plays a major role on the global magnetic behavior of Co_2TiO_4 system [33]. Such random anisotropy originates mainly in unsystematic lattice distortions which screen the local charge fluctuations due to large charge difference between the electronic configurations of Co^{2+} and Ti^{4+} [33].

The ac-magnetic susceptibility $\chi_{ac}(T)$ studies by Srivastava *et al*. reveals few multiple transitions in Co_2TiO_4 below 20 K which are related to the 'Gaby and Toulouse' type mixed phases T_{M1} and T_{M2} [34, 35]. The $\chi_{ac}(T)$ measurements performed in the presence of low dc-bias field dependence ($0 \leq H_{DC} \leq 150$ Oe) for frequency $f = 21$ Hz show the first transition at 16.5 K due to a transition from paramagnetic to a spin-glass state, which disappears as the dc-bias field approaches to 150 Oe [34]. In 1975, Sherrington and Kirkpatrick (SK) first established the theoretical study for such reentrant spin-glass behavior in spinels using mean-field approach [41-43]. Later, Gabay and Toulouse extended the SK Ising model calculations to the vector spin-glasses and showed that it is possible to have multiple phase transitions such as: magnetically ordered state $\xleftrightarrow{T_C \text{ or } T_N}$ paramagnetic state $\xleftrightarrow{T_{M1}}$ mixed phase-1 $\xleftrightarrow{T_{M2}}$ mixed phase-2 [44-46]. The cation distribution and magnetic properties of series of spinels based on $Co_2Ge_xTi_{1-x}O_4$ ($0 \leq x \leq 1$) and $Co_{2-y}Zn_yTiO_4$ ($0 \leq y \leq 1$) was reported by Strooper *et al*. [30, 36]. For $x = y = 0$ they obtained the sublattice magnetizations $M_A(0) = 20450$ (G/cm^3)/mol and $M_B(0) = 19750$ (G/cm^3)/mol, $T_N \sim 53 \pm 2$ K, Curie constant $C = 5.4 \pm 0.1$ K cm^3/mol, and exchange constants $J_{AB} \sim -6.3 \pm 0.3$ K, $J_{AA} \sim -4.6 \pm 0.3$ K and $J_{BB} \sim -5.5 \pm 0.3$ K [30, 31, 36]. Recently, Nayak *et. al*. reported that the electronic state of Ti in Co_2TiO_4 is Ti^{3+} instead of Ti^{4+}, unlike the case of Co_2SnO_4 system where Sn^{4+} occupies the octahedral *B*-sites [22]. Using heat capacity, dc-magnetization and $\chi_{ac}(T)$ studies these authors reported that polycrystalline Co_2TiO_4 exhibit a quasi-long-range ferrimagnetic state below $T_N \sim 47.8$ K and a compensation temperature $T_{comp} \sim 32$ K together with giant sign reversible exchange bias at low temperatures [20,22,38]. Although a significant frequency dispersion was observed in $\chi_{ac}(T)$ of Co_2TiO_4, the mathematical analysis based on the Power-law of critical slowing down $\tau = \tau_o [(T_P/T_g) -1]^{-z\nu}$ yields a higher value of critical exponent $z\nu = 16$ as compared to $z\nu = 6.4$ for Co_2SnO_4 [22,25]. Usually, for a typical spin-glass system the magnitude of $z\nu$ should lie between 4 and 12 [49]. Therefore, the $\chi_{ac}(T)$ studies reported in references [22,38] reveal a lack of perfect spin–glass transition below T_N in

Co$_2$TiO$_4$ as compared to Co$_2$SnO$_4$ (T_{SG} = 39 K < T_N = 41 K) even though the ac-susceptibility data follows the A-T line behavior ($H^{2/3}$ vs T_P) [38].

On the other hand, previous studies on Co$_2$SnO$_4$ system reported that the longitudinal component of spins are responsible for the ferrimagnetic ordering below 41 K, and transverse component is accountable for the spin–glass state below 39 K, in which non-magnetic Sn^{4+} ions on the B sites are responsible for this disordered state [23,24]. Such coexistence of two magnetic phase transitions in Co$_2$SnO$_4$ are consistent with the semi spin-glass behavior predicted by Villain and the experimental observations of Srivastava et $al.$ [34,35,50]. Theoretical studies by Villain reveal that the long-range interactions between the canted local spins are responsible for the collective freezing of the transverse spin component at the spin-glass transition [50,51]. In all these studies, the samples are of polycrystalline in nature and no single-crystal study has been reported so far. Therefore, there is a need to pin down the spin configuration of Co$_2$TiO$_4$ and its sister compound Co$_2$SnO$_4$ precisely using neutron diffraction measurements below T_N which is the main objective of this article.

II. EXPERIMENTAL DETAILS

The single-crystalline sample of Co$_2$TiO$_4$ was prepared by the floating zone method. For this, the ceramic feed rod of Co$_2$TiO$_4$ sample was first prepared using the binary transition-metal oxide precursors; cobalt (II, III) oxide (Co$_3$O$_4$) and titanium dioxide (TiO$_2$) of 4N purity powders were taken in appropriate amounts and mixed in ethanol. These mixtures were calcined at 500ºC for 12 h in air and finally packed in a rubber tube of cylindrical geometry of 7 mm diameter and 100 mm length. These cylindrical samples were hydrostatically pressed at 2.5 kbars and sintered at 1350°C for 30 h in air (with 200°C/h heating and cooling rates) to obtain high density feed and seed rods for the floating zone growth. Small portions were cut-off from a feed rod and used for powder X-ray diffraction and magnetization measurements. The Co$_2$TiO$_4$ crystals have been grown by crucible-free floating zone method in air flow (500 ccm) using the four-mirror type image furnace (CSC, Japan) equipped with 1 kW halogen lamps. The pulling rate was maintained at 1.5-2.0 mm/h. The upper and lower shafts were counter rotated at 15 rpm, in order to suppress temperature fluctuations in the molten zone. The as-grown ingot was about 55-60 mm in length and about 6.5 mm in diameter with a metallic luster. The powder samples of Co$_2$SnO$_4$ have been prepared by standard solid-state-reaction method similar to the method given

in Ref [25]. Neutron powder diffraction experiments were carried out on a crushed Co_2TiO_4 single crystal using the instruments E2, E6, and E9 available at the BER II reactor of the Helmholtz-Zentrum Berlin. The instrument E9 uses a Ge-monochromator with neutron wavelength λ = 1.309 Å, while the instruments E2 and E6 use a pyrolytic graphite (PG) monochromator of neutron wavelengths λ = 2.38 Å and λ = 2.42 Å, respectively. On these instruments powder patterns were recorded between different ranges of diffraction angles: (*a*) 19.2 and 95.3° (E2), (*b*) 5.5 and 136.4° (E6), and (*c*) 5 and 141.8 ° (E9). On the instrument E2, neutron powder diffraction patterns of single-crystal Co_2TiO_4 and polycrystalline Co_2SnO_4 were collected at 1.6 (magnetically ordered regime) and 80 K (paramagnetic region) with very good counting statistics (24 h/pattern). In order to improve the instrumental resolution during the experiments we have used a 15 min collimator. The temperature dependence of magnetic ordering of both Co_2TiO_4 and Co_2SnO_4 has been investigated on the instrument E6.

The crystal and magnetic structures of cylindrical form of Co_2TiO_4 single-crystal of dimension *d* = 6.3 mm and *h* = 6.5 mm has been investigated on the four-circle diffractometer E5. The data were collected with a two-dimensional position sensitive ^{3}He-detector, 90 × 90 mm (32 × 32 pixels). The instrument E5 uses a Cu and PG monochromator selecting the neutron wavelengths λ = 0.896 and 2.39 Å, respectively. The shorter neutron wavelength has been used to collect a full data set to investigate in detail the crystal structure of Co_2TiO_4. For the investigation of the magnetic structure we have used the plane grating (PG) monochromator. For the investigation of the crystal structure at low temperature, a powder sample (crushed crystal) of Co_2TiO_4 was used. Neutron powder patterns were collected on the instrument E9 at 2 K and 60 K. Furthermore, we have followed the thermal variation of the intensity of prominent nuclear and magnetic Bragg reflections. The refinements of the crystal and magnetic structure were carried out with the *FullProf* suite [52]. In addition to this we have used the program *Xtal* 3.4 (Ref. [53]) for the refinements using the single-crystal data of Co_2TiO_4 collected at room temperature. For the absorption correction (Gaussian integration) we used the absorption coefficient μ = 0.75 cm^{-1}. Secondary extinction has been corrected using the formalism of Zachariasen (type I) and the following nuclear scattering lengths were used: $b(O)$ = 5.805 fm, $b(Ti)$ = 3.30 fm, $b(Co)$ = 2.50 fm, and $b(Sn)$ = 6.228 fm [54]. The magnetic form factors of the Ti^{3+}, Co^{2+} and Co^{3+} ions were taken from Ref. [55]. The ac-magnetic susceptibility (χ_{ac}) and dc-magnetization measurements (*M*) were performed using a superconducting quantum interference device (SQUID) based

magnetometer from Quantum-design with temperature capabilities of 2 - 320 K and magnetic field (H) up to ± 70 kOe. The low temperature heat capacity data was recorded by means of a physical property measurement system (PPMS) from Quantum Design.

III. RESULTS AND DISCUSSION

A. Crystal and Electronic structure

Figure 1 shows the neutron powder diffraction pattern of Co_2TiO_4 collected at temperatures between 1.6 K and 60 K together with their Rietveld refinement data. The calculated patterns (shown in red color) are compared with the experimentally observed data (shown in black circles). In the lower part of each diagram the difference pattern (shown in blue color) as well as the positions of the nuclear reflections of Co_2TiO_4 is shown. In the powder pattern collected at 1.6 K magnetic intensity appears at the position of the reflections $(111)_M$. It is well known that the inverse spinel Co_2TiO_4 crystallizes in the cubic space group $Fd\bar{3}m$ (No. 227, cell choice 2). Usually, in normal spinels with the general formula AB_2O_4 the A^{2+} ions are located on the tetrahedral site (A site), while the B^{3+} ions are located on the octahedral site (B site). In Co_2TiO_4 cobalt occurs in two valence states as Co^{2+} and Co^{3+} [22]. Therefore, it can be expected that Co^{2+} occupy the A site and Co^{3+} occupy one half of the B site. Consequently, the titanium ions have the trivalent state and they statistically occupy the other half of the B site. The formula of this inverse spinel can be given as $Co(Co_{0.5}Ti_{0.5})_2O_4$. In order to check the correctness of the chemical composition we have investigated the detail crystal structure of Co_2TiO_4. At room temperature no additional reflections could be detected, which clearly indicated that the F centering and the d-glide planes are not lost. For the refinements a total of 1680 (94 unique) reflections were collected in the 2θ range from 5.3 to 48.6°. Due to the vastly different scattering lengths of the titanium and cobalt atoms we were able to determine the occupancies of these atoms with good accuracy. For the A site and B site the metal atoms are located at the Wyckoff positions $8b(\frac{3}{8},\frac{3}{8},\frac{3}{8})$ and $16c(0,0,0)$, while the O atoms are located at the position $16e(x,x,x)$. During the refinement we allowed to vary the following parameters: (i) the overall scale and extinction factor g, (ii) the positional parameter x of the O atom, and (iii) the isotropic thermal parameters of the Ti and Co atoms as well as the anisotropic thermal parameters U_{11} (= U_{22} = U_{33}) and U_{12} (= U_{13} = U_{23}) of the O atom. For the A and B sites we have used the constraint

$occ(Ti) + occ(Co) = 1$. Further we have used the constraint for the isotropic thermal parameters U of the atoms of the A and B sites. This is due to the fact, that the scattering power of the B site is strongly reduced by a partial compensation of the positive and negative scattering lengths of the Co and Ti atoms. However, the refinements resulted in a satisfactory residuals $R_F = 0.043$ defined as $R_F = \sum(||F_o^2| - |F_c^2||) / \sum|F_o^2|$. For the A site we have obtained the occupancies $occ(Ti) = -0.031(16)$ and $occ(Co) = +1.031(16)$. This clearly shows that the A site is fully occupied with Co^{2+} ions. On the other hand, the occupancies of the B site were found to be $occ(Ti) = 0.513(8)$ and $occ(Co) = 0.487(8)$. These are very close to the expected values of 0.5. Thus, our investigation does affirm the highly unusual oxidation state of Ti ions (+3) in the crystal structure of Co_2TiO_4 phase when prepared in air. For the extinction parameter g, which is related to the mosaic distribution, we obtained the value $g = 929(113)$ rad^{-1}. The results of the refinements are summarised in Table I.

In order to investigate the structural properties at low temperature we have collected neutron powder diffraction data on E9 at 1.6 and 60 K (Fig. 1), in the magnetically ordered regime as well as in the paramagnetic region. In Fig. 1 it can be seen that additional intensity occurs at the position of the reflection 111 due to a ferrimagnetic ordering at 1.6 K, which will be discussed in detail in the following section. Furthermore, in the low-temperature powder pattern we could not found any peak splitting or broadening. Therefore, within the instrumental resolution we cannot find a transition to a lower symmetric structure. For example, the normal spinel $NiCr_2O_4$ shows a transition from the cubic space group $Fd\overline{3}m$ to tetragonal one with the space group $I4_1/amd$ followed by another transition into an orthorhombic structure with the space group $Fddd$ [56]. A refinement in the next lower symmetric space group $I4_1/amd$ resulted in lattice parameters $a_{orth} = a_{tet} \sqrt{2} = 8.4402(14)$ Å, and $c_{orth} = c_{tet} \sqrt{2} = 8.4416(29)$ Å. Further, in Table 1 it can be seen, that the changes of the refined parameters are negligible from 297 K down to 1.6 K. Interestingly, our single-crystal data showed, that the thermal variation results in a strong change of the intensity of strong nuclear reflections (Fig. 2). The strong increase of the 400 reflection of about 65 % (from 60 K down to 8 K) cannot be purely ascribed to an increase of magnetic intensity. From our powder data collected on E2 the increase is only 16 %. In this case the increase in the intensity of the neutron powder diffraction peak 400 can be purely ascribed to a onset of the magnetic ordering, because of the absence of secondary extinction. On the contrary, for the single crystal one can clearly confirm the presence of extinction effects from the crystal structure refinements

as discussed above. Such effect can be ascribed to a change of the orientation of mosaic blocks in the single crystal caused by strain effects and results in an increased broadening of Bragg reflections with decreased extinction. Since the extinction coefficients '*y*' refer to the reductions in F^2 ($y \sim F_{obs}^2/F_{cal}^2$) the intensities of the strongest reflections are significantly affected. Moreover, for the reflection 222, which is at 60 K even stronger than the 400, this effect is much less pronounced. Here we found an increase of only 7 and 14 % from the powder (E2) and the single-crystal diffraction (E5) experiments, respectively. This indicates that the change of mosaicity (or extinction) is anisotropic at low temperature. This effect was also observed by a high-resolution synchrotron powder diffraction study of $Ni_{0.85}Cu_{0.15}Cr_2O_4$, where a strong peak broadening was observed for the 400, whereas the reflection 222 remains unchanged [56]. Thus, the strong anisotropic strain broadening is essentially based on competing Jahn-Teller effects acting along different crystallographic axes. For the Co^{2+} ions at the *A* site, which have the $3d^7$ configuration, cooperative distortions of the CoO_4 tetrahedra through the Jahn-Teller effect should be absent. Nevertheless, electronic energy could be gained for the Ti^{3+} and Co^{3+} ions having the $3d^1$ and $3d^6$ configurations, respectively. For both ions the $2t_g$ levels are expected to split into a lower d_{xy} level and a higher twofold generate d_{xz}/d_{yz} level. Thus, one would expect for both ions tetragonal distortions with a *c*/*a* ratio smaller than 1. From the refined tetragonal lattice parameters of Co_2TiO_4 in the space group $I4_1/amd$ as given above we obtained a *c*/*a* ratio of 1.0002(7), which is practically equal to 1. On the other hand it has to be mentioned that the reflection 400 measured at 1.6 K was found to be slightly broader than that measured at 60 K (*FWHM* from 0.414 to 0.429°). A similar trend shows the reflection 222 (*FWHM* from 0.423 to 0.440°). However, the observed *FWHM* values practically represent the instrumental resolution. Therefore, the *FWHM* of the reflection 222 is slightly larger than that of the 400. This confirms that a tetragonal splitting is hardly to detect from our powder data, since a significant peak broadening should only expected for the reflection 400 (into 400/040 and 004). For comparison the reflection 400, measured in our single-crystal experiment, was found to be even broader (*FWHM* = 0.73°) taking into account the instrumental resolution ($FWHM_{sam} = \sqrt{FWHM_{obs}^2 - FWHM_{Instr}^2}$). As discussed above the intrinsic peak broadening can be ascribed to a rougher orientation of mosaic blocks in the single crystal. Due the worse resolution of the PG monochromator and the intrinsic peak broadening no change of the peak width is observable between 8 and 80 K. Furthermore, it is important to note that Co_2TiO_4 does not show a

spontaneous structural phase transition could not be observed, which is in agreement with our neutron powder data. In Fig. 2 it can be seen, that such a transition is smeared out due to the structural disorder in this material. However, extinction effects can give us additional information about the increase of anisotropic strain effects, which are locally induced by the Jahn-Teller effect in the Co_2TiO_4 single crystal.

In order to determine the electronic state of all the ions present in the single crystal Co_2TiO_4 systems, we performed the X-ray photoelectron spectroscopy (XPS) measurements with Al-K_α X-rays as source. Figure 3 shows the photoelectron intensity of the sample versus binding energy (eV) of the core level spectra of (a) Co-^2p (b) Ti-^2p and (c) O-1s, and (d) Co-^2p (e) Sn-^3d and (f) O-1s for Co_2TiO_4 single crystal and Co_2SnO_4 polycrystal, respectively. We noticed two major peaks at 780.58 eV and 795.68 eV associated with the spin-orbit splitting ($^2p_{3/2}$ and $^2p_{1/2}$ levels) which are further deconvoluted into four peaks at 780.35 eV(P_1), 782.26 eV(P_2), 795.85 eV(P_3) and 797.26 eV(P_4) signifying the presence of Co^{3+} state [Doublet: P_2–P_4] in addition to the Co^{2+} [Doublet: P_1–P_3]. In addition, three weak broad satellite peaks were noticed at 773.46 eV (S_1), 785.84 eV (S_2) and 802.45 eV (S_3). Usually, the energy splitting (ΔE) between the two levels due to spin-orbit coupling should be different for the divalent and trivalent Co ions with ΔE = 15.7 eV and 15.0 eV for Co^{2+} and Co^{3+}, respectively [57-59]. In the present case for Co_2TiO_4 single crystal the separations between the doublet peaks found to be ΔE_{P1-P3} = 15.5 eV and ΔE_{P2-P4} = 15 eV corresponding to the Co^{2+} and Co^{3+} respectively. On the other hand, the highest intensity peak for Ti-$^2p_{3/2}$ centered at 457.93 eV, together with this peak we noticed a second peak across 463.75 eV corresponding to Ti-$^2p_{1/2}$ (Fig. 3b). Usually, Ti ions exhibit tetravalent oxidation state in most of the oxides; for example, in TiO_2 the binding energy separation for doublets of Ti $\Delta[^2p_{3/2}-^2p_{3/2}]$ = 5.7 eV, however, in the present case the $\Delta[^2p_{3/2}-^2p_{3/2}]$ = 5.82 eV signifying the presence of Ti^{3+}. The observed position of the peak at 457.93 eV agrees with the previously reported data of Ti^{3+} surface defects in TiO_2 system [60]. Moreover, our observations rule out the presence of any metallic 'Ti' ions in Co_2TiO_4 matrix which usually show their signatures in XPS spectra at 454 eV [59]. Figure 3c shows the core level spectra of O-1s which requires a minimum of three Gaussian-Lorentzian peaks to reproduce the experimentally observed XPS spectra. These deconvoluted peaks are centered at 530.03 eV, 532.20 eV and 533.63 eV signifying the presence of surface oxygen, metal-ligand bonding and excess oxygen present in the system [57-59,62-64]. On the contrary, the Co-^2p XPS spectrum (Fig. 3d) for Co_2SnO_4 deconvoluted only

into two major peaks at 780.6 eV and 796.3 eV, with satellite peaks at 786.15 eV and 802.4 eV. The binding energy seperation ΔE between the two major peaks ($^2p_{3/2}$ and $^2p_{1/2}$) is 15.7eV, which confirms the presence of divalent oxidation state of Co $i.e.$ Co^{2+}, and no additional signatures for the Co^{3+} state are observed in Co_2SnO_4. Figure 3(e) shows the Sn-3d core level XPS spectrum for Co_2SnO_4 which exhibits sharp peaks at 485.65 eV and 494.8 eV and a weak shoulder at 496.75 eV signifying the presence of the Sn^{4+} state. The O-1s XPS spectra (Fig. 3(f)] shows the characteristics of Co–O lattice oxygen and surface oxygen.

As compared to the single crystal O-1s core level spectra there is a significant asymetric peak broadening was noticed which may be associated with the presence of increase in surface oxygen vancancies [65]. Usually, polycrystalline samples contains many grain boundaries and dislocations as compared to the singlecrystalline sample. Moreover, in polycrystalline cobalt orthotitanate the peak positions are shifted towards higher binding energy (and an additional peak at 527.8 eV) due to the significant role of electronegativity (since the oxygen ions are linked with different electronic states of cobalt and titanium ions) [66]. On the contrary, in cobalt orthostannate the oxygen ion is bonded with only divalent cobalt ions at both tetrahedral A and octahedral B sites and tetravalent stannus ions, therefore electronegativity plays a small role) [66]. From this analysis we observed that Co_2TiO_4 single crystals exhibits electronic structure (give as $(Co^{2+})[Co^{3+}Ti^{3+}]O_4$) similar to that of the polycrystalline samples reported recently.

B. Microscopic magnetic moments and magnetic structure

For a detailed understanding of the magnetic order in Co_2TiO_4 we have collected the powder patterns on the instruments E2 and E6. It has already been mentioned above that Co^{2+} occupy the A site, and the magnetic ions Ti^{3+} and Co^{3+} statistically the B site. Complementary to this study we also have investigated the magnetic ordering of Co_2SnO_4 to separate out the individual contributions of the Co^{2+} and Co^{3+} ions. In this compound the B site is occupied with magnetic Co^{2+} and diamagnetic Sn^{4+} ions. Neutron powder diffraction patterns of Co_2TiO_4 and Co_2SnO_4 were collected at 1.6 and 80 K on the instrument E2. In Fig. 4 it can be seen, that the intensities of the nuclear Bragg reflections are significantly different for Co_2TiO_4 as compared to Co_2SnO_4. This can be ascribed to the strongly different scattering lengths of the Ti and Sn atoms. The refinements of structural parameters at 80 K resulted in satisfactory residuals of $R_F = 0.031$ (Co_2TiO_4) and $R_F = 0.014$ (Co_2SnO_4). In contrast, the difference patterns of both compounds

(Fig. 4) look very similar indicating that their magnetic structures are practically the same. Here all magnetic intensities were found to be on the positions of allowed nuclear Bragg reflections, which indicate a ferrimagnetic ordering between the atoms located at the tetrahedral and octahedral sites. Figure 4 shows that for both the strongest magnetic intensities can be observed at the position of the reflection 111. The only difference arises through the presence of the magnetic reflection $(200)_M$ in the powder pattern of Co_2TiO_4, which is forbidden for the cubic space group $Fd\bar{3}m$. Thus, the presence of this reflection suggests a loss of at least one of the *d*-glide planes resulting in an additional antiferromagnetic ordering with a moment direction perpendicular to the ferrimagnetic ones. Magnetic intensity of the $(200)_M$ can be generated, if the moments of the Co1(Ti) atoms at the positions (1) 0,0,0; (2) ¾,¼,½; (3) ¼.½,¾; (4) ½,¾,¼ show the spin sequences $+--+$, $+-+-$, and $++--$. Due to the fact, that the reflection $(200)_M$ could only be observed for Co_2TiO_4 the existence of an additional antiferromagnetic ordering in Co_2SnO_4 can be excluded. A similar type of ordering was found for the Cu-rich chromites in the system $Ni_{1-x}Cu_xCr_2O_4$ [5]. In both spinel types one finds strong exchange interactions between the atoms located at the tetrahedral and octahedral sites resulting in a ferrimagnetic spin alignment. For the chromites, where orthorhombic distortions (space group *Fddd*) are strongly pronounced, the ferri- and antiferromagnetic components were found to parallel to the *a* and *c* axis, respectively. Further it has to be mentioned that in $NiCr_2O_4$ the ferrimagnetic and the antiferromagnetic transition sets in at two different magnetic transition temperatures, where the magnetic ordering can be described with two different propagation vectors [5].

In contrast to the system $Ni_{1-x}Cu_xCr_2O_4$, we cannot distinguish the difference between the three cubic axes of Co_2TiO_4 and Co_2SnO_4. For the Co^{2+} ions (in our case Co2) at the *A* site, which have the $3d^7$ configuration ($e_g{}^4$, $t_{2g}{}^3$), cooperative distortions of the CoO_4 tetrahedra through the Jahn-Teller effect should be absent. Assuming a high-spin state three unpaired electrons in the t_{2g} level give a magnetic moment $\mu_{eff} = g \cdot S = 3.0$ μ_B. On the other hand, electronic energy could be gained for the Ti^{3+} and Co^{3+} ions (in our case Co1) having the $3d^1$ ($t_{2g}{}^1$, $e_g{}^0$) and $3d^6$ ($t_{2g}{}^4$, $e_g{}^2$) configurations, respectively. For both ions the t_{2g} levels are expected to split into a lower d_{xy} level and a higher twofold generate d_{xz}/d_{yz} level. Here Ti^{3+} has one and Co^{3+} has four unpaired electrons and accordingly one expects magnetic moments $\mu_{eff} = 1.0$ μ_B and $\mu_{eff} = 4.0$ μ_B, respectively. Therefore, we have used in the refinements, as described in detail below, of Co_2TiO_4 a constraint $\mu(Co^{3+}) = 4\,\mu(Ti^{3+})$.

Interestingly, in Fig. 4 it can be seen that the magnetic peak $(111)_M$ of both Co_2TiO_4 and Co_2SnO_4 is much broader than the nuclear one 111 observed for Co_2SnO_4. The Rietveld refinements of the powder patterns of both Co_2TiO_4 and Co_2SnO_4 (collected on E2) resulted in the best fit for the nuclear reflections, where a pure Gaussian profile was used. In contrast, for the magnetic reflections, a pure Lorentzian resulted in the best fit. Usually, the diffraction profiles of both the nuclear and magnetic reflections are expected be the same. The origin of the peak broadening of the magnetic $(111)_M$ reflection in the powder pattern may be related to the disorder of the Ti and Co cations at the B site, which form perfect-crystal microdomains (called magnetic mosaic blocks) leading to a Lorentzian distribution. On the other hand, the absence of secondary extinction in the powder diffraction data signifies the fact that the magnetic moments are not perfectly ordered. Usually in the case of a perfect three-dimensional magnetic order, one would expect the similar peak profiles as observed in the case of nuclear ones. The cause of this effect might be the statistical distribution of the Co and Ti/Sn atoms at the B site. Therefore, one can assume that a part of the moments shows a partial disorder in a so-called spin-glass state (the ac-magnetization dynamics discussed later provides further evidence to the existence of spin-glass state in the Co_2TiO_4 single crystals). In order to estimate the degree of 3-dimensional magnetic ordering we have deduced the correlation lengths (defined as $\xi = 1/HWHM$) from the strongly broadened magnetic reflection $(111)_M$. For Co_2TiO_4, where the magnetic reflection $(111)_M$ is much stronger pronounced that the nuclear one 111, we could obtain from the neutron powder data the correlation length $\xi \sim 15$ Å. For comparison, the obtained correlation length $\xi \sim 20$ Å, obtained from the single-crystal data, was found to be somewhat larger. However, in the present study we have used the integrated magnetic intensities of both Co_2TiO_4 and Co_2SnO_4 to estimate the magnitude of the magnetic moments (μ). The results of the refinements are summarized in Fig. 4 and Table II. For the Co^{2+} and Co^{3+} ions one finds three and four unpaired electrons, respectively. Assuming a spin-only system the expected theoretical magnetic moments ($\mu_{eff} = g\,S\,\mu_B$) are $\mu_{eff} = 3.0\ \mu_B$ (Co^{2+}) and $\mu_{eff} = 4.0\ \mu_B$ (Co^{3+}). Assuming Co^{2+} on the A site and Co^{3+} on the B site it can be seen for that the experimental moments are somewhat reduced, where one finds for Co1 atoms on the B site $\mu_{tot}(Co1) = 3.17(5)\ \mu_B$ (E2) and $\mu_{tot}(Co1) = 2.94(6)\ \mu_B$ (E6), and for the Ti atoms $\mu_{tot}(Ti) = 0.79(2)\ \mu_B$ (E2) and $\mu_{tot}(Ti) = 0.74(2)\ \mu_B$ (E6). For Co2 on the A site the moments are $\mu_{tot}(Co1) = 1.62(4)\ \mu_B$ (E2) and $\mu_{tot}(Co1) = 2.11(4)\ \mu_B$ (E6). Due to the much better counting statistics on E2 we were able to determine the z component of Co1/Ti

with better accuracy. Here we found the values $\mu_x(Co1) = 0.89(9)$ μ_B and $\mu_x(Ti) = 0.22(2)$ μ_B. For Co_2SnO_4 the strongest magnetic intensity was also found at the position of the reflection 111. In Fig. 4 it can be seen the nuclear intensity of the 111 of Co_2SnO_4 is rather strong, whereas in the case of Co_2TiO_4 it was negligible. Therefore, the magnetic moments could not be determined with same accuracy as those of Co_2TiO_4. Interestingly for Co_2SnO_4 no intensity could be observed on the position of the reflection 200 (as shown in Fig. 4), suggesting the absence of an additional antiferromagnetic component. Due to this reason we were not able to determine the temperature dependence of magnetic moments of Co_2SnO_4 precisely from our E6 experimental data. Therefore, in Fig. 5 we only present the temperature dependence of the magnetic moments of the cobalt and titanium atoms in Co_2TiO_4. Below the ferrimagnetic Néel temperature T_N ~ 48.6 K (estimated from $\partial(\chi_{DC}T)/\partial T$ vs. T as shown in the supplementary Fig. 1s of Ref. [67]) the magnetic moments of Co1 and Ti atoms located at the B sites are coupled antiparallel to the moments of the Co2 atoms located at the A site. During the refinement we have used a moment ratio $\mu(Co^{3+})/\mu(Ti^{3+}) = 4$. As well as the moment direction parallel to the 'a' axis.

Moreover, in order to obtain the effective magnetic moment μ_{eff}, the temperature dependence of inverse paramagnetic susceptibility curves $\chi_{ZFC}^{-1}(T)$ ($\chi_{ZFC} = M_{ZFC}/H$) (Fig. 2s of Ref. [67]) for Co_2TiO_4 single-crystal and poly-crystal are fitted to the experimental data with the Néel's expression for ferrimagnets viz. $1/\chi = (T/C) + (1/\chi_0) - [\sigma_0/(T - \theta)]$ [68]. A systematic comparison of all the fitting parameters including the molecular field constants (N_{AA}, N_{AB} and N_{BB}) and exchange constants (J_{AA}, J_{AB} and J_{BB}) obtained from the above analysis for Co_2TiO_4 single and polycrystalline samples are listed in Table III. The effective magnetic moment $\mu_{eff} = 7.526$ μ_B/f.u. of Co_2TiO_4 is determined by using the relation $C = N\mu_{eff}^2/3k_B$. Since the tetrahedral co-ordination does not allow orbital contribution, the magnetic moment at A-site of Co^{2+} ions is fixed as $\mu(A) = 3.87$ μ_B with spin $S = 3/2$ and $g = 2$ and $\mu(B) = 6.46$ μ_B is determined using the formula $\mu_{eff}^2 = [\mu(A)]^2 + [\mu(B)]^2$ for Co_2TiO_4 single crystal which yields ferrimagnetism below 'T_N' with net small moment of 2.59 μ_B/f.u. and these values are greater (1.32 μ_B) than their polycrystals. The experimentally obtained value $\mu_{eff} = 7.526$ μ_B for Co_2TiO_4 single crystal is slightly larger (1.04 μ_B per f.u.) than the theoretically predicted value $\sqrt{[(3.87\mu_B)^2]_{A=Co^{2+}} + [(1.73\mu_B)^2]_{B=Ti^{3+}} + [(4.9\mu_B)^2]_{B=Co^{3+}}} = 6.48$ μ_B. This is due to the significant role of orbital contribution of the cations occupying the octahedral sites. Note that in the present case the trivalent titanium ions Ti^{3+} with its $3d^1$ electronic configuration has magnetic

moment $\mu = 1.73$ μ_B. Considering the magnetic moment of Ti^{3+}, $\mu_{eff} = 7.526$ μ_B and $\mu(A) = 3.87$ μ_B our calculation yields the total moment of $\mu(Co^{3+}) \sim 6.218$ μ_B, which is greater than its spin-only moment 4.9 μ_B signifying the orbital contribution (1.318 μ_B) in the octahedral sites. On the contrary, no such orbital contribution was noticed for the polycrystalline Co_2TiO_4 which exhibits $\mu_{eff} = 6.5$ μ_B/f.u. and is less than the μ_{eff} obtained for single-crystal but higher than the isostructural compound Co_2SnO_4. The important difference between the Co_2TiO_4 and Co_2SnO_4 is that the B sites are occupied by trivalent Co and trivalent Ti in Co_2TiO_4 both of which exhibits non-zero magnetic moment, however, non-magnetic tetravalent Sn and divalent Co fills the octahedral B sites in Co_2SnO_4. Consequently, the effect of magnetic dilution is expected to be very less in Co_2TiO_4 as compared to its sister compound Co_2SnO_4. The strength of the antiferromagnetic exchange coupling between the two Co^{2+} spins on the tetrahedral 'A' and octahedral 'B' sites is often termed as asymptotic Curie temperature $T_a = C/\chi_0$. The corresponding values of T_a are 202.48 K and 125.18 K for single crystal and polycrystalline Co_2TiO_4, respectively. Another key feature of Co_2TiO_4 is the observation of compensation effect at T_{COMP} $\sim$ 30.4 K below the ferrimagnetic ordering temperature.

In order to confirm the spin-glass behavior a detailed frequency dependence (0.17 Hz $\leq f$ $\leq$ 1200 Hz) of ac-magnetic susceptibility studies were performed. Figure 6 shows the temperature dependence of real- and imaginary-components of $\chi_{ac}(T)$ ($= \chi'(T) + i \chi''(T)$) for different values of 'f'. For these measurements the peak-to-peak amplitude of ac-magnetic field h_{ac} is set to $\sim$ 4 Oe with negligible H_{DC}. It is clearly evident that the peak maximum (T_P) in $\chi'(T)$ shifts towards higher temperature side with increasing the frequency which is a typical characteristic of spin-glass system. To examine such property, the variation of T_P with-respect-to

f has been analyzed using the dynamic scaling-law given by the equation $\tau = \tau_0 \left(\dfrac{T_P - T_F}{T_F} \right)^{-zv}$

[69,70]. In this equation τ_0 is related to the relaxation of the individual cluster magnetic moment ($\tau_0 = 1/2\pi f_o$ is the value of attempt frequency), 'T_F' is the spin-glass transition temperature, 'z' is the dynamical critical exponent and 'v' is the critical exponent of correlation length. The scattered points shown in Fig. 7(a) shows the logarithmic variation of T_P as a function of 'τ' and the straight lines represents the least square fits (ln [τ] against ln[($T_P - T_F$)/T_F]) to the T_P data obtained from $\chi_{ac}(T)$. This fitting analysis yields the following parameters for the single crystal of Co_2TiO_4: $f_o = 3.746 \times 10^{25}$ Hz, $T_F = 46.85$ K and 'zv' = 12.04 $\pm$ 0.05 for $T_P(\chi')$ and $f_o = 3.746 \times 10^{16}$

Hz, T_F = 41.59 K and 'zv' = 2.17 ± 0.05 for T_P (χ''). The magnitudes of 'f_o' and 'zv' are consistent with the glassy characteristics of prototype spin-glasses reported in literature [68-71]. On the contrary, our earlier report dealing with the polycrystalline Co_2TiO_4 samples shows zv > 16 indicate the departure from a proper spin-glass nature [22]. In particular, the magnitude of $f_o \simeq$ 10^{16} Hz corresponds to spin-flip frequency of magnetic moments of ions or atoms [69,71,75,76].

We also analyzed the frequency dispersion of χ_{ac}(T) data with the Vogel-Fulcher law which is usually expressed as $\tau = \tau_0 \exp\left(\dfrac{E_a}{k_B(T - T_0)}\right)$; where τ_0 is the relaxation time constant (τ_0 = $1/2\pi f_o$ is the characteristic frequency of the clusters), T_0 is a measure of the interaction between magnetic clusters, k_B is the Boltzmann constant and E_a is the activation energy or the potential barrier separating two adjacent clusters [69,71-76]. The solid-lines in Fig. 7b represents the best fits corresponding to the above discussed Vogel-Fulcher law to the experimental data points obtained from $\chi_{ac}(T)$. This exercise yields T_0 = 46.86 K (41.52 K) and f_0 = 1.081 × 10^{15} Hz (1.07 × 10^{15} Hz) for $\chi'(\chi'')$. Usually, the large values of f_0 has been seen in other spin-glass systems as well, for example AgMn, CuMn, and AuFe which indicates the presence of interacting magnetic spin clusters of significant sizes in the investigating system [69,71,72,75,76]. The competition between ferrimagnetism and magnetic frustration in the system is the main source of existence of spin clusters which leads to a short-range order occurring just below T_N. Earlier investigations on the magnetic properties of $Y_{0.7}Ca_{0.3}MnO_3$ and $La_{0.96-y}Nd_yK_{0.04}MnO_3$ (0 ≤ y ≤ 0.4) reported the formation of such spin-clusters with short-range order [73,74]. Another important gauge to understand the nature of the spin-glass freezing processes is that the determination of relative shift (Φ) of the peak temperature per decade frequency using the expression Φ = $\Delta T_p/(T_p \Delta \log f)$, where ΔT_P is the change in T_P with change in log f [77,78]. Consequently, we have calculated the values of Φ = 0.0044 and 0.0052 using χ' versus T and χ'' versus T, respectively. Usually, Φ parameter should lie between 0.005 and 0.05 for typical spin-glasses. Thus, the values of Φ estimated from both real- and imaginary components of χ_{ac}(T) are consistent with the literature data on spin-glass ordering and is supporting the scaling analysis discussed above. Further evidence to the spin-glass behavior in Co_2TiO_4 single crystals was noticed from the temperature dependence of heat-capacity $C_P(T)$ (Fig. 3s of Ref. [67]). The fact that peak in 'C_P' at 'T_N' in H = 0 is quite weak compared to peaks observed in typical second order transitions in 3D systems is due to unconventional ordering in Co_2TiO_4 (lack of proper long-range order and the presence of

spin-glass-like features). Therefore, the absence of sharp peak in the $C_P(T)$ is a well-known characteristic feature of the existence of disordered spin configuration and proof to the existence of spin-glass nature [76].

The temperature variation of C_P/T (Fig. 3s of Ref. [67]) for $T < 100$ K for $H_{dc} = 0$, 1 and 5 T suggests the entropy loss due to spin-glass-like ordering starting near to T_{P2} (supplementary data in Fig. 1s and 3s of Ref. [67]). The zero-field $C_P T^{-1}$ data shows a weak hump across the T_N (= T_{P2}) and without any signatures across the compensation point T_{COMP}. However, after applying the field a sharp transition across T_{COMP} emerged with complete suppression of the hump observed across T_{P2}. There is a one-to-one concurrence between the location of these anomalies and the sharp transitions noticed in $\chi_{dc}(T)$ data at 48.18 K and 30.4 K. Nevertheless, no significant measurable difference was observed in the C_P values measured at $H = 0$ and 5 T except the emergence of T_{COMP} and disappearance of weak anomaly across T_N. Nonetheless, a rapid decrease in $C_P T^{-1}$ with decreasing T beginning near 25 K (a hump across 18 K), indicating further changes in the magnetic ordering of the system. These anomalies are clearly evident in the computed plots of differential magnetic entropy $\partial S_M / \partial T$ versus T curves.

It is well known that in magnetic materials the total specific heat $C_P(T)$ consists of two main components: The first one is due to lattice specific heat (C_L) and the second contribution is from magnetic counterpart (C_M). The lattice contribution consists of the electronic part C_e and the phonon part $C_{Phonon} = N f_D(\Theta_D/T) = 9 N R (T/\Theta_D)^3 \int_0^{\frac{\theta_D}{T}} \frac{x^4 e^x}{(e^x-1)^2} dx$, where $f_D(\Theta_D/T) = 9R$ $(T/\Theta_D)^3 \int_0^{\frac{\theta_D}{T}} \frac{x^4 e^x}{(e^x-1)^2} dx$ is the single Debye function, N is the number of atoms per formula unit, R is the universal gas constant (8.314 J/mol K), and Θ_D is the Debye temperature [42]. Usually, the electronic contribution is significant only at very low temperatures, the phonon contribution has been extracted from the total specific heat. For this we have fitted the experimentally obtained heat capacity data using Debye function [$f_D(\Theta_D/T)$] at temperatures much higher than the T_N where the magnetic contribution vanishes [80]. For the single crystalline Co_2TiO_4 the extrapolate data is shown in the inset of Fig. 3s in Ref. [67]. The solid continuous line depicts the contribution of the phonon and the solid-circles represents the magnetic-specific heat component individual derived from the above relation. Consequently, we obtained $\Theta_D = 554.16$ K which is higher than the $\Theta_D = 525$ K pure Co_3O_4 reported by Roth but consistent with the polycrystal data and are in close agreement with $\Theta_D = 560$ K reported by Ogawa and Waki for Co_2TiO_4 [42,81].

Furthermore, the temperature variation of the $\partial S_M/\partial T$ (= C_{MP}/T) exhibit a hump across 18 K and a sharp peak across the T_{COMP} of Co_2TiO_4 at high fields ($\geq$ 1 T) typical for a first-order-like transitions, however, this field-dependent anomaly is not sharp at low fields. Previous studies from Ogawa and Waki reveals that the $C_P(T)$ data of Co_2TiO_4 follows the simple $T^{3/2}$ dependence in a narrow range of temperatures whereas, the modified $T^{3/2}$ dependence (according to the equation C_M = ($k_B/8$)($k_BT/\pi\hbar a)^{3/2}$ $F(x)$)) was noticed over a wide range of temperature (5 - 30 K). The effective anisotropy constant K_a (~1.2×10^5 erg/cc) estimated by them is less than K_a = 9.3×10^5 erg/cc obtained from the present case (at T = 10 K).

Extensive ac-magnetization studies on polycrystalline Co_2TiO_4 and Co_2SnO_4 reported by Srivastava et al. observed four different transitions in the $\chi_{ac}(T)$ data recorded in the presence of small probing external dc-magnetic field in the range 285 - 460 Oe with f = 21 Hz and V_{p-p} ~ 0.5 Oe [34,35]. The first two transitions and their field dependence given in these reports are in-line with the two transitions observed in the $\chi_{ac}(T)$ data (Fig. 8) of Co_2TiO_4 single crystals measured in the same temperature window as that of frequency dependence studies discussed above, however, with a superimposition of a small fixed dc-bias field H_{dc} =10, 20 and 30 Oe similar to that reported in Ref [22]. Figure 8 shows the $\chi'(T)$ and $\chi''(T)$ measured at various H_{dc} with fixed f = 2 Hz with H_{ac} = 4 Oe. The amplitude of both $\chi'(T)$ and $\chi''(T)$ decreases significantly (~88%) with increasing the H_{DC} by 0.2 %, nevertheless, two peaks are clearly evident in $\chi'(T)$ curves (inset of Fig. 8) with the extent of splitting increases with increase of H_{dc}. This behavior is consistent with the two-peak scenario of differential dc-magnetic susceptibility shown in the supplementary data (inset of Fig. 1s of Ref. [67]). Since the out-of-phase component of the $\chi_{ac}(T)$ is related with the transverse spin component, the current observations supports the co-occurrence of ferrimagnetism in the longitudinal spin component at T_N and spin-glass ordering of the transverse spin component at a slightly lower temperature across T_F. Such phenomenon of semi-spin-glass state was predicted in the papers by Gabay and Toulouse and Villain in insulators with non-magnetic impurities [46,50,51].

IV. SUMMARY

The structural and magnetic properties of Co_2TiO_4 and Co_2SnO_4 were investigated by powder and single-crystal neutron diffraction. Complementarily the temperature dependence of heat-capacity, dc-magnetization and ac-susceptibility was measured. Both compounds exhibit

strongest magnetic intensity for the $(111)_M$ reflection due to ferrimagnetic ordering. Also, a low intensity magnetic reflection $(200)_M$ was noticed in Co_2TiO_4 due to additional weak antiferromagnetic ordering. A significant broadening of the $(111)_M$ reflection has been observed due to the disordered character of the Ti and Co atoms on the B site. The neutron diffraction study of Co_2TiO_4 single-crystals showed that some nuclear reflections exhibit a strong increase in their peak intensity below the ordering temperature of about 50 K which is associated to a change of the mosaicity of the crystal. The cause of anisotropic local strain effects in the crystal appears due to the competing Jahn-Teller effects acting along different crystallographic axes in which the t_{2g} levels of both the trivalent cations Ti^{3+} and Co^{3+} split into a lower d_{xy} level resulting to a higher twofold degenerate d_{xz}/d_{yz} level. As a consequence, one can expect a tetragonal distortion in Co_2TiO_4 with a c/a ratio less than 1. However, our powder diffraction data could not evidence any peak splitting, which could indicate a transition into a tetragonal structure. Based on the dynamic scaling analysis of ac-susceptibility and the heat-capacity measurements, it is suggested that Co_2TiO_4 first goes through a ferrimagnetic ordering across 48.6 ± 1 K, and then subsequently goes through a reentrant spin-glass transition across 46.8 K with critical exponent 'zv' = 12.04 ± 0.05 as determined from the frequency dependence of real-component of ac-magnetic susceptibility $\chi'(T)$. From the temperature dependence of heat-capcity $C_P(T)$ data we estimated the Debye temperature $\Theta_D = 554.16$ K for the single crystalline Co_2TiO_4 which is significantly higher than the $\Theta_D = 525$ K for polycrystalline Co_3O_4 reported by Roth [81]. A weak hump across 18 K was noticed from the $C_P T^{-1}$ vs. T data indicating further change in the magnetic ordering which is independent of the external applied magnetic field.

References

[1] R. E. Camley, Z. Celinski, T. Fal, A. V. Glushchenko, I. R. Harward, V. Veerakumar, and V. V. Zagorodnii, J. Magn. Magn. Mater. **321**, 2048 (2009).
[2] M. Fujishima, IEICE Electron. Express **6**, 721 (2009).
[3] Y. Naito and K. Suetake, IEEE Trans. Microw. Theory Tech. **19**, 65 (1971).

[4] K. Tomiyasu, J. Fukunaga, and H. Suzuk, Phys. Rev. B **70**, 214434 (2004); J. Lee, S. Bae, Y. Hong, J. Jalli, G. Abo, W. Seong, S. Park, C. Choi, and J. Lee, J. Appl. Phys. **105**, 07A514 (2009).

[5] Y. Yamasaki, S. Miyasaka, Y. Kaneko, J.-P. He, T. Arima, and Y. Tokura, Phys. Rev. Lett. **96**, 207204 (2006); K. Hanashima, Y. Kodama, D. Akahoshi, C. Kanadani, and T. Saito, J. Phys. Soc. Jpn. **82**, 024702 (2013).

[6] S. Thota and S. Singh, in *Magnetic Spinels-Synthesis, Properties and Applications* (In Tech, 2017).

[7] P. Dutta, M. Seehra, S. Thota, and J. Kumar, J. Phys.: Condens. Matter **20**, 015218 (2007).

[8] S. Thota, A. Kumar, and J. Kumar, Mater. Sci. Eng., B **164**, 30 (2009).

[9] S. Singh, P. Pramanik, S. Sangaraju, A. Mallick, L. Giebeler, and S. Thota, J. Appl. Phys. **121**, 194303 (2017).

[10] F. Guillou, S. Thota, W. Prellier, J. Kumar, and V. Hardy, Phys. Rev. B **83**, 094423 (2011).

[11] T. Zou, Y.-Q. Cai, C. R. dela Cruz, V. O. Garlea, S. D. Mahanti, J.-G. Cheng, and X. Ke, Phys. Rev. B **94**, 214406 (2016).

[12] A. Miyata, S. Takeyama, and H. Ueda, Phys. Rev. B **87**, 214424 (2013).

[13] S. Abiko, S. Niidera, and F. Matsubara, Phys. Rev. Lett. **94**, 227202 (2005).

[14] S. B. Roy and M. K. Chattopadhyay, Phys. Rev. B **79**, 052407 (2009).

[15] S. Niidera and F. Matsubara, Phys. Rev. B **75**, 144413 (2007).

[16] T. Sato, T. Ando, and T. Ogawa, S. Morimoto and A. Ito, Phys. Rev. B, **64**, 184432 (2001).

[17] P. Pramanik, S. Thota, S. Singh, D. C. Joshi, B. Weise, A. Waske, and M. Seehra, J. Phys: Condens. Matter **29**, 425803 (2017).

[18] R. Padam, T. Sarkar, R. Mathieu, S. Thota, and D. Pal, J. Appl. Phys. **122**, 073908 (2017).

[19] D. Mandrus, V. Keppens, and B. Chakoumakos, Mater. Res. Bull. **34**, 1013 (1999).

[20] S. Nayak, D.C. Joshi, M. Krautz, A. Waske, J. Eckert, S. Thota, J. Appl. Phys, **119**, 043901 (2016).

[21] R. Padam, S. Pandya, S. Ravi, A. K. Nigam, S. Ramakrishnan, A. K. Grover, D. Pal, Appl. Phys. Lett. **102**, 112412 (2013).

[22] S. Nayak, S. Thota, D. C. Joshi, M. Krautz, A. Waske, A. Behler, J. Eckert, T. Sarkar, M. S. Andersson, R. Mathieu, V. Narang, and M. S. Seehra, Phys. Rev. B **92**, 214434 (2015).

[23] S. Thota and M. Seehra, J. Appl. Phys. **113**, 203905 (2013).

[24] S. Thota and M. Seehra, J. Appl. Phys. **118**, 129901 (2015).

[25] S. Thota, V. Narang, S. Nayak, S. Sambasivam, B. Choi, T. Sarkar, M. Andersson, R. Mathieu, and M. Seehra, J. Phys.: Condens. Matter **27**, 166001 (2015).

[26] I. Fita, A. Wisniewski, R. Puzniak, V. Markovich, G. Gorodetsky. Phys. Rev. B **93**, 184432 (2016).

[27] R. Kumar, R. Padam, S. Rayaprol, Vasudeva Siruguri, D. Pal, J. Appl. Phys,**119**, 12 (2016).

[28] S. Thota, F. Guillou, V. Hardy, A. Wahl, W. Prellier, and J. Kumar, J. Appl. Phys. **109**, 053902 (2011).

[29] S. Thota, K. Singh, S. Nayak, C. Simon, J. Kumar, and W. Prellier, J. Appl. Phys. **116**, 103906 (2014).

[30] K. De Strooper, A. Govaert, C. Dauwe, and G. Robbrecht, Phys. Status Solidi A **37**, 127 (1976).

[31] K. De Strooper, Phys. Status Solidi A **39**, 431 (1977).

[32] J. Hubsch and G. Gavoille, Phys. Rev. B **26**, 3815 (1982).

[33] G. Gavoille, J. Hubsch, and S. Koutani, J. Magn. Magn. Mater. **102**, 283 (1991).

[34] J. Srivastava, S. Ramakrishnan, V. Marathe, G. Chandra, R. Vijayaraghavan, J. Kulkarni, V. Darshane, and S. Singh, J. Appl. Phys. **61**, 3622 (1987).

[35] J. Srivastava and J. Kulkarni, J. Phys. C: Solid State Phys. **20**, 2139 (1987).

[36] K. De Strooper, A. van Alboom, C. Henriet-Iserentant, R. Vanleerberghe, R. Vandenberghe, Phys. Status Solidi A **44**, 215 (1977).

[37] S. Nayak, K. Dasari, D. Joshi, P. Pramanik, R. Palai, V. Sathe, R. Chauhan, N. Tiwari, S. Thota, Phys. Status Solidi B **253**, 2270, (2016).

[38] S Nayak, K Dasari, DC Joshi, P Pramanik, R Palai, A Waske, RN Chauhan, N. Tiwari, T. Sarkar, S. Thota, J. Appl. Phys. **120**, 163905, (2016).

[39] M. Ingaki and S. Naka, J. Solid State Chem. **13**, 365 (1975).

[40] M. A. Prosnikov, A. D. Molchanova, R. M. Dubrovin, K. N. Boldyrev, A. N. Smirnov, V. Yu. Davydov, A. M. Balbashov, M. N. Popova, R. V. Pisarev, Phys. Solid State **58**, 2516 (2016) [Fiz. Tverd. Tela **58**, 2427 (2016)].

[41] N. Sakamoto and Y. Yamaguchi, J. Phys. Soc. Jpn. **17**, 276 (1962); **17**(Suppl. B1) 276 (1962).

[42] S. Ogawa and S. Waki, J. Phys. Soc. Jpn. **20**, 540 (1965).

[43] S. B. Kirkpatrick and D. Sherrington, Phys. Rev. B **17**, 4384 (1978).

[44] D. Sherrington, Phys. Status Solidi B **251**, 1967 (2014), D. Sherrington and S. Kirkpatrick, Phys. Rev. Lett. **35**, 1792 (1975).

[45] J. Jayaprakash and S. Kirkpatrick, Phys. Rev. B **21**, 4072 (1980).

[46] M. Gabay and G. Toulouse, Phys. Rev. Lett. **47,** 201(1981).

[47] R. Galazka, S. Nagata, and P. Keesom, Phys. Rev. B **22**, 3344 (1980).

[48] D. M. Cragg, D. Sherrington, and M. Gabay, Phys. Rev. Lett. **49**, 158 (1982).

[49] K. Binder and A. P. Young, Rev. Mod. Phys, **58**, 801 (1986); J. Mydosh, Hyperfine Interact. **31**, 347 (1986).

[50] J. Villain, Z. Phys. B **33**, 31 (1979).

[51] J. Villain, R. Bidaux, J.-P. Carton, R. Conte, J. Phys. **41**, 1263 (1980).

[52] J. Rodríguez-Carvajal, Physica B (Amsterdam) **192**, 55 (1993).

[53] S. R. Hall, G. S. D. King, J. M. Stewart, eds., *The Xtal3.4 User's Manual*. (Lamb Print, University of Western Australia, Perth, 1995).

[54] V. F. Sears, in *International Tables for Crystallography*, edited by A. J. C. Wilson (Kluwer Academic Publishers, Dordrecht/Boston/London, 1995), C, 383.

[55] P. J. Brown, in *International Tables for Crystallography*, edited by A. J. C. Wilson (Kluwer Academic Publishers, Dordrecht/Boston/London, 1995), C, 391.

[56] M. Reehuis, M. Tovar, D. M. Többens, P. Pattison, A. Hoser, and B. Lake, Phys. Rev. B **91**, 024407 (2015).

[57] J. K. Kwak, K. H. Park, D. Y. Yun, D. U. Lee, T.W. Kim, D. I. Son, J. H. Han, and J. Y. Lee, J. Korean Phys. Soc. **57**, 1803 (2010).

[58] J.-G. Kim, D. Pugmire, D. Bhattagila, and M. A. Langell, Appl. Surf. Sci. **165**, 70 (2000).

[59] S. C. Petitto, E. M. Marsh, G. A. Carson, and M. A. Langell, J. Mol. Catal. A: Chem. **281**, 49 (2008).

[60] E. McCafferty and J. L. Wightman, Surf. Interface Anal. **26**, 549 (1998).

[61] M. C. Biesinger, L. W. Lau, A. R. Gerson and R. S. C. Smart, Appl. Surf. Sci. **257** 887 (2010).

[62] Y. Fu, H. Du, S. Zhang, and W. Huang, Mater. Sci. Eng. A **403**, 25 (2005).

[63] J. Xu, P. Gao, and S. T. Zhao, Energy Env. Sci. **5**, 5333 (2012).

[64] P. N. Shelke, Y. B. Khollam, K. R. Patil, S. D. Gunjal, S. R. Jadkar, M. G. Takwale, and K. C. Mohite, J. Nano. Electron. Phys. **3**, 486 (2011).

[65] L. Aswaghosh, D. Manoharan, and N. V. Jaya, Phys. Chem. Chem Phys. **18**, 5995 (2016).

[66] Z. Zhou, Y. Zhang, Z. Wang, W. Wei, W. Tang, J. Shi, and R. Xiong, Appl. Surf. Sci. **254**, 6972 (2008).

[67] See Supplement Material at http:/link..aps.org/supplemental/10.1103/Phys.RevB.144104 for temperature dependence of magnetization, inverse susceptibility and specific heat of single crystal Co_2TiO_4.

[65] A. H. Morrish, *The Physical Principles of Magnetism* (Wiley-VCH, 2001), p. 696.

[66] T. Sarkar, V. Duffort, V. Pralong, V. Caignaert, and B. Raveau, Phys. Rev. B **83**, 094409 (2011).

[67] J. Tholence, Solid State Commun. **35**, 113 (1980).

[68] J. Souletie and J. L. Tholence, Phys. Rev. B **32**, 516 (1985).

[69] A. Harris and R. Fisch, Phys. Rev. Lett. **38**, 796 (1977).

[70] R. Mathieu, P. Nordblad, D. N. H. Nam, N. X Phuc, and N. V. Khiem, Phys. Rev. B **63**, 174405 (2001).

[71] R. Mathieu, P. Svedlindh, and P. Nordblad, Europhys. Lett. **52**, 441(2000).

[72] R. Brand, H. Georges-Gibert, J. Hubsch, and J. Heller, J. Phys. F: Met. Phys. **15**, 1987 (1985).

[73] C. P. Poole and H. A. Farach, Z. Phys. B **47**, 55 (1982).

[74] M. S. Seehra and K. L. Pisane, J. Phys. Chem. Solids **93**, 79 (2016).

[75] K. L. Pisane, E. C. Despeaux and M. S. Seehra, J. Mag. Mater. **384**, 148-154 (2015).

[76] R. Mathieu, J. P. He, Y. Kaneko, H. Yoshino, A. Asamitsu, and Y. Tokura, Phys. Rev. B **76**, 014436 (2007).

[77] E. Gopal, *Specific heats at low temperatures, International Cryogenics Monograph series* (1966).

[78] W. Roth, J. Phys. Chem. Solids **25**, 1 (1964).

TABLE I. Results of the refinements of the single-crystal (sc) neutron diffraction study of Co_2TiO_4 collected on E5 at 297 K. The refinement of the crystal structure was carried out in the cubic space group $Fd\bar{3}m$ (cell choice 2). The thermal parameters U_{ij} (given in 100 Å^2) are in the form $\exp[-2\pi^2(U_{11}\,h^2a^{*2} + \ldots 2U_{13}\,hla^*c^*)]$. For symmetry reasons one finds for the O atom $x = y = z$, $U_{11} = U_{22} = U_{33}$, and $U_{12} = U_{13} = U_{23}$. In the lower part of the Table the positional and isotropic thermal parameter of the O atoms are given as obtained from the neutron powder diffraction study (pc) on E9 at 1.6 and 60 K, respectively.

E5, sc	$Fd\bar{3}m$	x	y	z	U_{11}	U_{12}
$Co2^{2+}$	$8b$	⅜	⅜	⅜	0.51(7)	-
$Ti^{3+}/Co1^{3+}$	$16c$	0	0	0	0.51	-
O	$32e$	0.24002(11)	0.24002	0.24002	1.06(5)	−0.23(2)

Lattice parameter: a = 8.4440(4) Å at 297 K, R_F = 0.043

E9, pc	$Fd\bar{3}m$	x	y	z	U_{is}	
$Co2^{2+}$	$8b$	⅜	⅜	⅜	0.80(2)	
$Ti^{3+}/Co1^{3+}$	$16c$	0	0	0	0.80	
O (at 60 K)	$32e$	0.23937(6)	0.23937	0.23937	1.07(2)	
$Co2^{2+}$	$8b$	⅜	⅜	⅜	0.79(2)	
$Ti^{3+}/Co1^{3+}$	$16c$	0	0	0	0.79	
O (at 1.6 K)	$32e$	0.23941(6)	0.23941	0.23941	1.04(2)	

Lattice parameter: a = 8.4413(2) Å at 1.6 K, R_F = 0.047; a = 8.4421(2) Å (60 K), R_F = 0.062

TABLE II. Magnetic moments (in μ_B) of the Co and Ti atoms in Co_2TiO_4 and Co_2SnO_4 at 1.6 K as obtained from the refinements using the neutron diffraction data collected on the instruments E2 and E6. In the space group $Fd\bar{3}m$ (cell choice 2) the magnetic Co1(Ti) atoms are located at the positions (1) 0,0,0; (2) ¾,¼,½; (3) ¼.½,¾; (4) ½,¾,¼; while the Co2 atoms are located at (1) ⅜,⅜,⅜; (2) ⅛,⅝,⅛, respectively. The ferrimagnetically (FI) and antiferromagnetically (AF) coupled moments are lying orthogonal to each other.

Moment	Co_2TiO_4, E2	Co_2TiO_4, E6	Co_2SnO_4, E2	Co_2SnO_4, E6
$\mu(Co1)$, FI	3.04(6)	2.89(6)	2.57(11)	2.18(11)
$\mu(Ti)$, FI	0.76(2)	0.72(2)	-	-
$\mu(Co1)$, FI	0.89(9)	0.55(17)	-	-
$\mu(Ti)$, AF	0.22(2)	0.14(4)	-	-
$\mu_{tot}(Co1)$	3.17(5)	2.94(6)	2.57(11)	2.18(11)
$\mu_{tot}(Ti)$	0.79(2)	0.74(2)	-	-
$\mu(Co2)$, FI	1.62(4)	2.11(4)	2.04(7)	1.97(6)
R_M	0.058	0.083	0.060	0.124

TABLE III: The list of various parameters obtained from the Néel fits of χ^{-1}_{ZFC} versus T curve recorded under zero-field-cooled condition for both single-crystal and polycrystalline Co_2TiO_4.

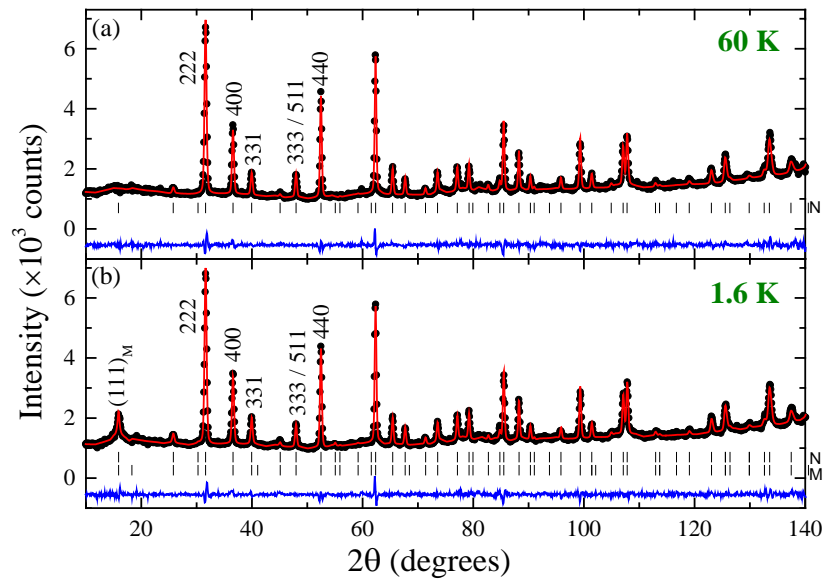| Systems	C (emu K mol⁻¹Oe⁻¹)	χ_0 (emu mol⁻¹Oe⁻¹)	σ_0 (emu⁻¹Oe mol K)	θ (K)	μ_{eff} (μ_B)	μ (A) (μ_B)	μ (B) (μ_B)
Co_2TiO_4 (Single-crystal)	7.087	0.035	99.812	46.736	7.526	3.87	6.46
	N_{AA}	N_{BB}	N_{AB}	J_{AA}	J_{BB}	J_{AB}	
	63.453	41.372	84.385	11.979 k_B	12.312 k_B	14.656 k_B	
Co_2TiO_4 (Poly-crystal)	5.245	0.0419	31.55	49.85	6.5	3.87	5.19
	N_{AA}	N_{BB}	N_{AB}	J_{AA}	J_{BB}	J_{AB}	
	17.319	12.720	35.700	3.25 k_B	4.47 k_B	3.18 k_B	

Figures

FIG. 1. (color online) Rietveld refinements of the neutron powder diffraction data of Co_2TiO_4 collected at 1.6 K and 60 K. The crystal structure was refined in the cubic space group $Fd\bar{3}m$. The calculated patterns (red) are compared with the observed one (black circles). In the lower part of each diagram the difference pattern (blue) as well as the positions of the nuclear reflections of Co_2TiO_4 are shown. In the powder pattern collected at 1.6 K magnetic intensity appears at the position of the reflections 111.
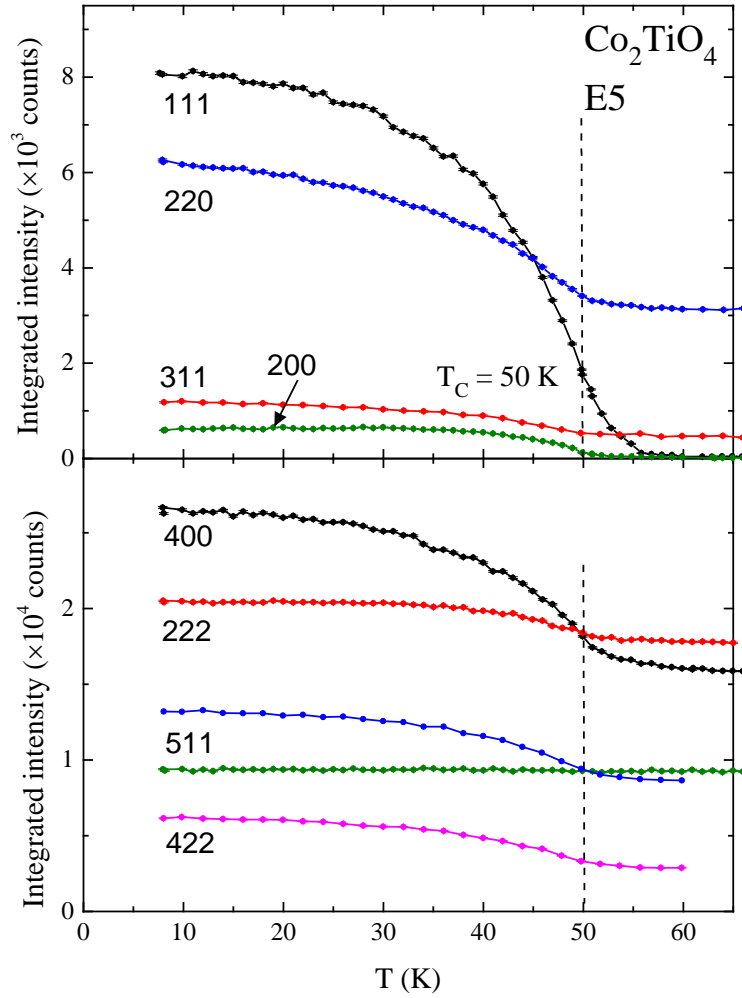
FIG 2. (color online) Temperature dependence of nuclear and magnetic Bragg reflections of Co_2TiO_4 single crystal. The strongest magnetic intensity shows the reflections 111, which is increasing well above Curie temperature T_C = 50 K. The presence of the magnetic reflection 200 can be ascribed to an additional weak antiferromagnetic ordering. The strong increase of the 400 indicates the existence of anisotropic change of the mosaicity in the crystal.
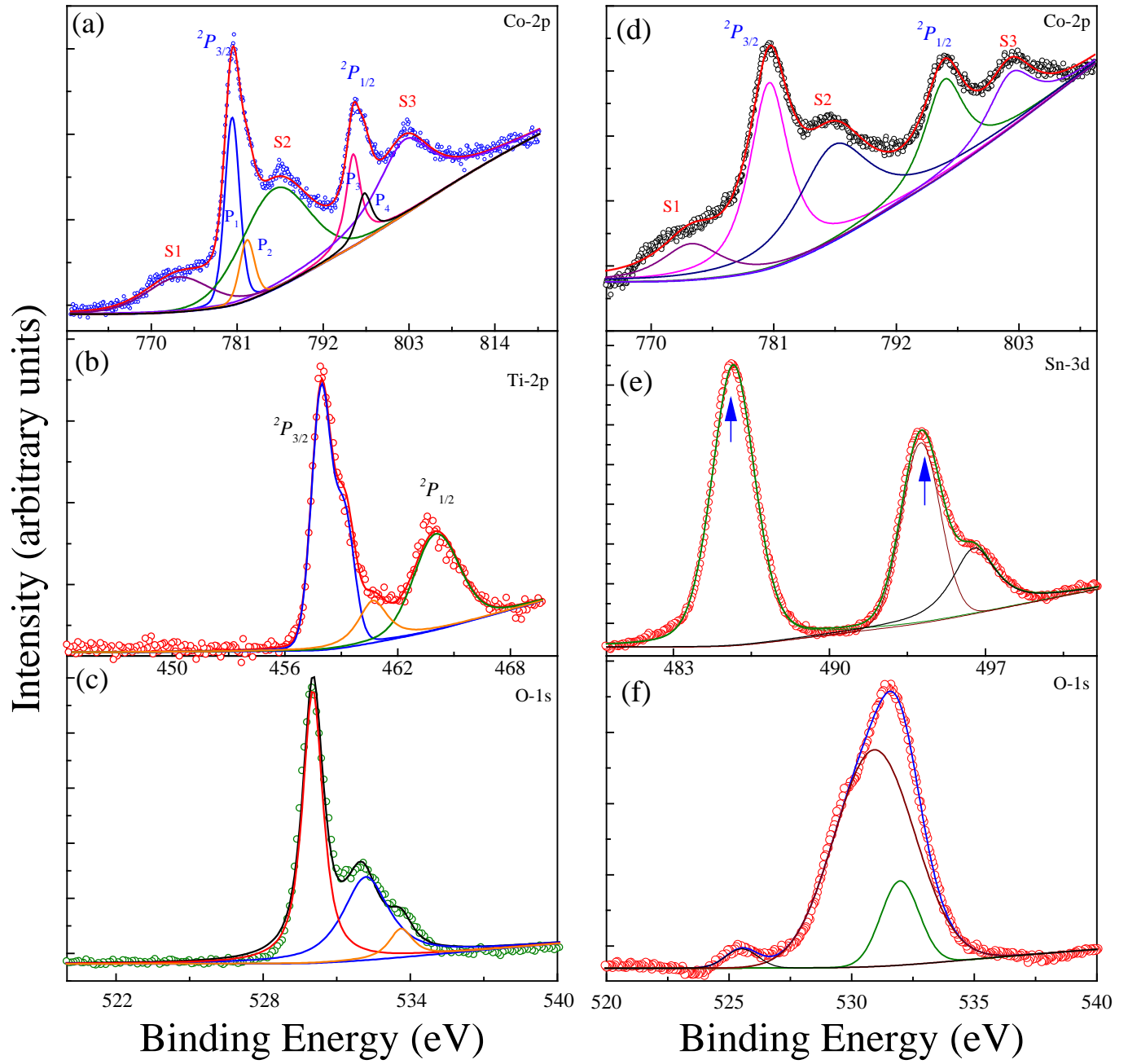
FIG. 3. The X-ray photoelectron spectra (XPS) of (a) Co-2p, (b) Ti-2p and (c) O-1s peaks of single crystal Co_2TiO_4 and (d) Co-2p, (e) Sn-3d and (f) O-1s peaks of polycrystalline Co_2SnO_4.
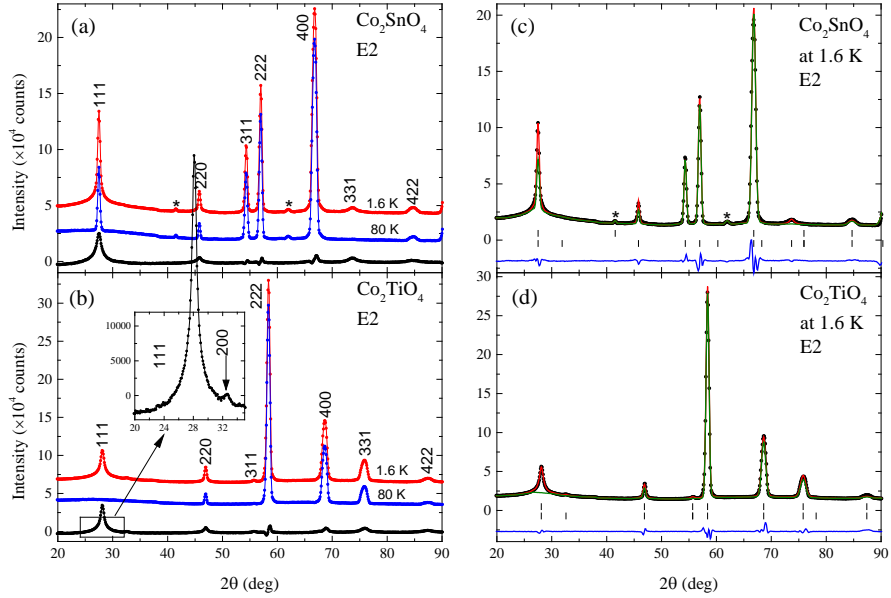
FIG 4. (color online) Neutron powder patterns of (a) Co_2SnO_4 and (b) Co_2TiO_4 at 1.6 (blue) and 80 K (red) collected on the instrument E2. Due to the vastly different scattering lengths of the Ti and Sn atoms the intensities of the nuclear reflections of Co_2TiO_4 and Co_2SnO_4 strongly differ. In contrast, the difference patterns (black) of both compound are very similar indicating that the magnetic ordering is practically the same. The only difference arises through the presence of the magnetic reflection $(200)_M$ in the powder pattern of Co_2TiO_4. The observed and calculated powder patterns of (c) Co_2SnO_4 and (d) Co_2TiO_4 as obtained from Rietveld refinements are compared in the right part of the figure. The calculated patterns (red) are compared with the observed one (black circles). In the lower part of each diagram the difference pattern (blue) as well as the positions of the nuclear reflections of Co_2TiO_4 are shown. For comparison the calculated of the pure nuclear part (green) is also shown. The sample of Co_2SnO_4 contains a small impurity of SnO_2. The positions of the strongest reflections are marked with stars.
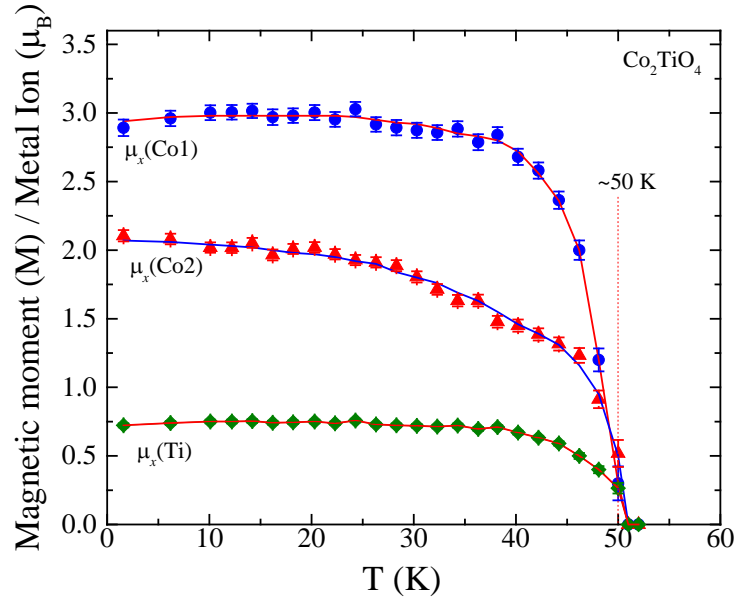
FIG. 5. Temperature dependence of magnetic moments of the cobalt and titanium atoms in Co$_2$TiO$_4$. Below the Curie temperature T_C = 50 K the magnetic moments of Co1 and Ti atoms located at the B site are coupled antiparallel to the moments of the Co2 atoms located at the A site. During the refinement we have used a moment ratio $\mu(Co^{3+})/\mu(Ti^{3+})$ = 4. As well as the moment direction parallel to the a axis.
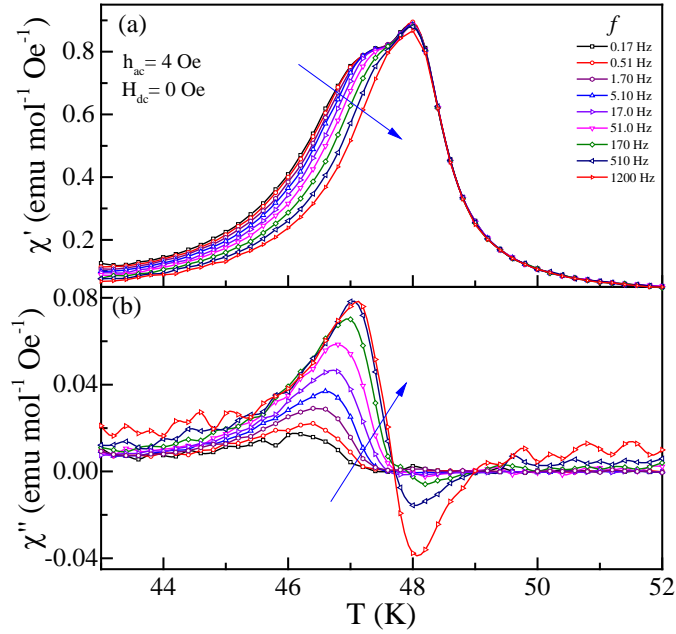
FIG. 6. Temperature dependence of ac-magnetic susceptibility of Co_2TiO_4 single crystal (a) real component $\chi'(T)$, and (b) imaginary $\chi''(T)$ components measured at various frequencies between 0.17 Hz and 1200 Hz under warming condition using ac-peak-to-peak amplitude $H_{ac}= 3$ Oe without any external dc-magnetic field.
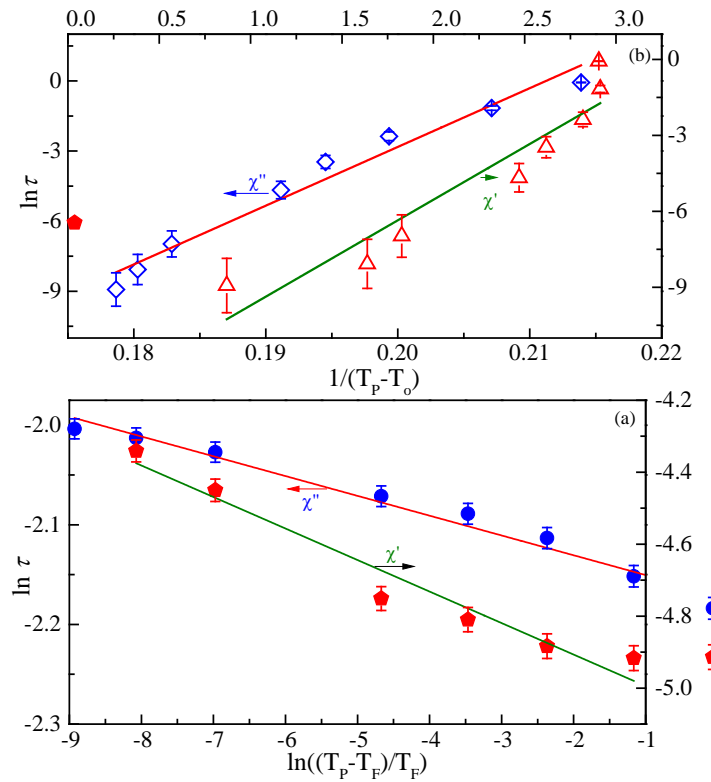
FIG. 7. (a) The logarithmic variation of the peak-temperature obtained from $\chi'(T)$ and $\chi''(T)$ (i.e. Power law analysis ln $[\tau]$ versus ln($[T_P - T_F]/T_F$)) the solid line represents the best fit to the experimental data. (b) Plots associated with the Vogel-Fulcher law ln $[\tau]$ versus $[1/(T_P - T_o)]$ using the peak positions in $\chi'(T)$ and $\chi''(T)$ and the solid lines shows the best-fit to experimental data.
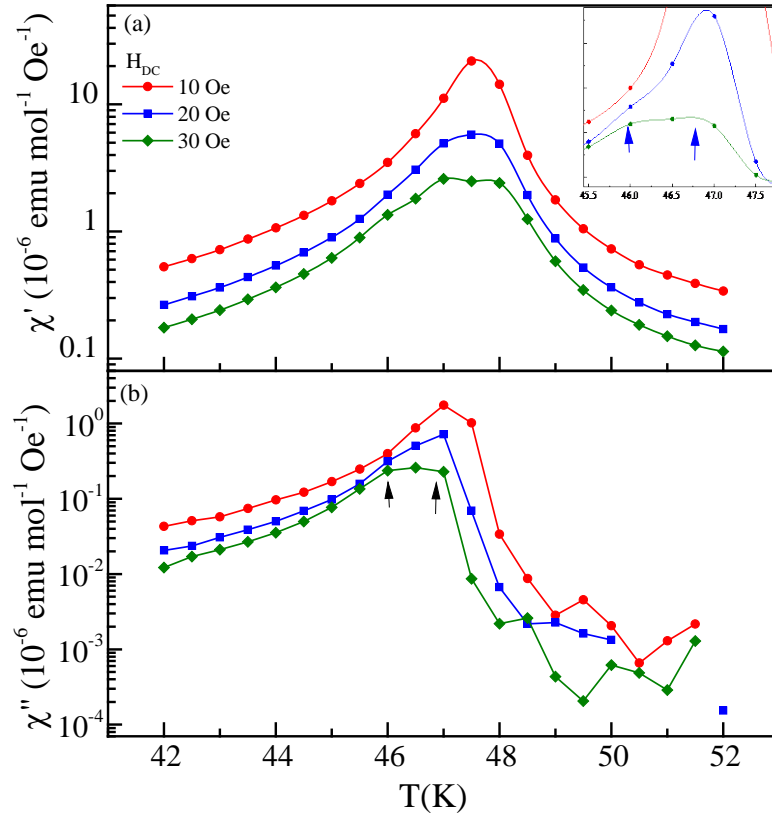
FIG. 8. Temperature dependence of ac-magnetic susceptibility (a) real part $\chi'(T)$, and (b) imaginary $\chi''(T)$ components of single crystalline Co_2TiO_4 system measured at three different bias fields H_{dc} (10, 20 and 30 Oe) at a constant frequency of 2 Hz and ac-magnetic field peak-to-peak amplitude of 4 Oe. The inset shows peak splitting in $\chi'(T)$ which is significant at higher values of H_{dc}.